Real-time braking control based on optic flow divergence onboard an underwater vehicle

Lucia Bergantin, Christophe Viel, Luc Jaulin

Real-time braking control based on optic flow divergence onboard an underwater vehicle

Lucia Bergantin*, Christophe Viel**, Luc Jaulin*

** L.B. and L.J. are with ENSTA-Bretagne, Robex, Lab-STICC, Brest, France. email: lucia.bergantin@ensta-bretagne.fr, ** C.V. is with CNRS, Lab-STICC, ENSTA-Bretagne, F-29806, Brest, France. email: christophe.viel@gadz.org*

ARTICLE INFO

Keywords:
Obstacle avoidance, underwater navigation, optic flow

ABSTRACT

Obstacle avoidance is a major challenge for underwater robot navigation, especially in cluttered environments where sonars are subject to reverberation and noise. Optic flow cues are widely used for aerial drone navigation, as they can be measured with broadly available sensors such as monocular cameras. Few studies have explored the possibility of using optic flow cues for underwater robot navigation, although this is more difficult due to imaging conditions and natural scene characteristics. In this study, we investigate the use of optic flow divergence for real-time collision avoidance onboard a Remotely Operated underwater Vehicle (ROV) equipped with monocular cameras. The measured optic flow divergence was first used to trigger an autonomous emergency braking response, then to estimate the relative distance of the underwater vehicle from the detected obstacle using an Extended Kalman Filter. This relative distance was used to maintain a predefined safe distance from the obstacle. Tests were first carried out in a pool, then in a harbour, in a lake and in the sea. Our findings show that this minimalistic method is effective under a wide range of visibility and turbidity conditions.

1. Introduction

Obstacle avoidance is a major challenge for the navigation of Unmanned Underwater Vehicles (UUVs). The robot must first be able to detect obstacles and then avoid them. In the underwater environment, limited visibility generally favours the use of sonar for obstacle detection. However, high-performance sonars are expensive, and can be particularly prone to interference in cluttered environments or near walls due to reverberation and noise. The resulting acoustic image is still useful for remote operators, but distance measurements are often very noisy and too unstable for automated position control systems in these conditions. In addition, the use of sonar is not always authorised (in the vicinity of military installations or near the coast, for example). Therefore, other solutions need to be considered.
Several approaches for UUV navigation involving the use of ArUco markers [27], acoustic systems [20], Simultaneous Localisation and Mapping (SLAM) methods [29, 28] or feature detection [5] have been proposed. Many of these approaches, however, require the fusion of outputs from several sensors. In cluttered environments, short-distance detection can be performed using electric sense [4] or vision.
Optic flow is a visual cue representing the apparent motion of objects, surfaces, and edges caused by the relative motion between an observer and a scene [6]. Optic flow cues are widely used for Unmanned Aerial Vehicle (UAV) navigation. Translational optic flow has been employed for controlled landing [22], uneven terrain following [9] and localization [14, 15]. Optic flow divergence has been used for visually controlled landing [11, 24, 8, 12], honeybee-inspired visual odometry [1] and obstacle avoidance [21, 26]. Methods for measuring optic flow divergence were tested onboard UAVs with a monocular camera for landing [8, 12] and optic flow sensors to perform odometry [1]. The optic flow divergence was also used to estimate the relative distance between a UAV and the ground using an Extended Kalman Filter (EKF) [1].
While optic flow has been extensively studied for aerial robotics, very few studies have explored the possibility of using optic flow cues for UUV navigation as well. A synthetic database of underwater scenes was presented to train Deep Neural Networks (DNN) for optic flow estimation [10]. Optic flow divergence resulting from depth variations has been employed to evaluate the scale factor of observed scenes to perform visual odometry onboard a Remotely Operated Vehicle (ROV) [7]. The use of optic flow for underwater navigation is much more challenging due to imaging conditions and natural scene characteristics: lack of visibility, illumination from artificial finite-energy sources that are installed on and move with submersible platforms in deep-water operations, medium attenuation according to color wavelengths, presence of floating particles, complex topographies of natural objects, etc... However, the results obtained in UAV navigation and the few UUV applications examined so far show the potential of optic flow for proximity navigation in cluttered environments, where other sensors such as sonar may fail.
ROVs are UUVs remotely controlled by operators on the surface. They are connected via a tether and can be equipped with cameras and other sensors for tasks like underwater inspections, data collection, and maintenance in deep and hazardous environments. Their field of application is vast, from dam inspection, offshore platform, and pipeline maintenance to marine research and underwater archaeology. Since ROV operators face practical challenges in proximity navigation due to complex underwater conditions (currents, lack of visibility,...), most works try to make robot control easier, more intuitive, and safer [23, 25].
In this study, we investigate the use of optic flow divergence

ORCID(s):

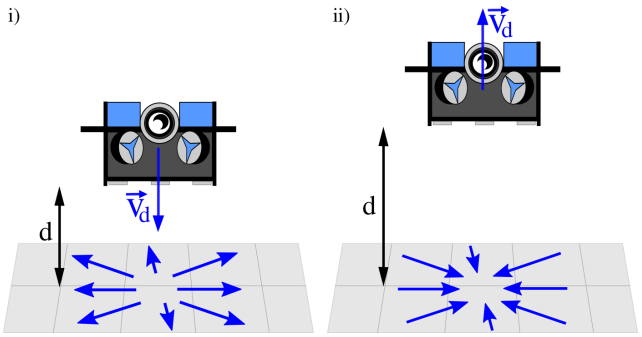

Figure 1: An expansion of the optic flow vector field is observed when a robot approaches a surface (i), while a contraction is observed when the robot moves away from it (ii).

for real-time minimalistic underwater collision avoidance onboard an ROV (referred to here as BlueBee robot). The presented approach is particularly suited for the avoidance of obstacles in close proximity. Optic flow divergence was measured using a monocular camera, building on the method presented in [12]. To our knowledge, it is the first time optic flow divergence is used for this purpose underwater. Additionally, the approach used in this study to measure optic flow divergence requires little computational power compared to other methods, such as DNN. The occurrence of an optic flow divergence measured during remote-controlled navigation was used to detect the presence of an obstacle and thus trigger an autonomous emergency braking response. The measured optic flow divergence was then used to estimate the relative distance of the BlueBee robot from the detected obstacle using an EKF. The estimated relative distance was employed to reach a predefined safe distance from the obstacle. Optic flow divergence was then continuously measured thanks to an imposed small oscillation, allowing the robot to maintain the predefined safe distance. To evaluate the proposed method under different conditions, tests were carried out in a pool, a harbour, a lake and in the Mediterranean sea.
To summarize, the main contributions of this work are:

- The presentation of an optic flow-based method for automatic braking response and distance estimation for proximity navigation, performed for the first time to our knowledge in an underwater environment,
- A minimalistic method to measure optic flow divergence underwater implemented in real-time on an ROV using a standard monocular camera,
- Tests performed in a pool and harbour with clear water, then in a lake with turbid water and finally in the sea.

2. The optic flow divergence

2.1. Definition of optic flow divergence

An expansion of the optic flow vector field is observed when approaching a surface, while a contraction is observed when moving away from it (see Figure 1). This series of expansions and contractions can be defined as the optic flow divergence ω_D. If we consider a robot equipped with a camera looking straight towards a surface, ω_D can be expressed as the ratio of the robot's velocity in the direction of the surface V_d to the robot's distance from the surface d:

$$\omega_D = \frac{V_d}{d} \tag{1}$$

2.2. Measurement in real-time onboard the BlueBee robot

In this study, we built on a method presented by previous authors to measure optic flow divergence with a monocular camera onboard a UAV for landing purposes [8, 12, 13]. Images were first converted from RGB to greyscale. At each time instant t, features n were detected with the Scale-Invariant Feature Transform (SIFT) algorithm [17, 18]. It should be noted that other detectors such as Features from accelerated segment test (FAST) (used in [8, 12, 13]) and Oriented FAST and rotated BRIEF (ORB) were tested, but both failed to detect enough features due to the lack of visual information underwater. SIFT was the only algorithm tested so far that was robust enough to detect a significant amount of features in order to measure optic flow divergence underwater. This was not a problem for previous authors (in [8, 12, 13]) because of the different environment. The detected features n were then converted to 2D points in the image plane. For each 2D point (u_i, v_i) we computed the distances $d_{ij}(t)$ with respect to every other point (u_j, v_j) on the image plane, as follows:

$$d_{ij}(t) = \sqrt{(u_i(t) - u_j(t))^2 + (v_i(t) - v_j(t))^2} \tag{2}$$

The 2D points were then tracked to the next image captured at time $t + \Delta t$ (with $\Delta t > 0$ a chosen time interval) with the Pyramidal Lucas Kanade method [3]. For each tracked 2D point (u_i, v_i) we computed the distances $d_{ij}(t + \Delta t)$ with respect to every other tracked point (u_j, v_j) on the image plane, as follows:

$$d_{ij}(t + \Delta t) = \sqrt{(u_i(t + \Delta t) - u_j(t + \Delta t))^2 + (v_i(t + \Delta t) - v_j(t + \Delta t))^2} \tag{3}$$

To compute the optic flow divergence ω_D at time $t + \Delta t$, we computed the ratios of $d_{ij}(t)$ and $d_{ij}(t + \Delta t)$ and took their average divided by Δt, as follows:

$$\omega_D(t + \Delta t) = \frac{1}{\Delta t} \frac{1}{N^2} \sum_{i=1}^{N} \sum_{j=1}^{N} \frac{d_{ij}(t + \Delta t) - d_{ij}(t)}{d_{ij}(t)} \tag{4}$$

with N the number of tracked 2D points.
Let us define:

- $\omega_{R,y}$ as the rotational optic flow component due to the rotation of the robot around the y axis of the camera (see Figure 2.ii),
- $\omega_{R,z}$ as the rotational optic flow component due to the rotation of the robot around the z axis of the camera.

To compensate for underwater currents and orientation instabilities due to remote operation, the higher of these two components was subtracted from the optic flow divergence, as follows:

$$\omega_D(t+\Delta t) = \begin{cases} \omega_D(t+\Delta t) - \omega_{R,y}(t+\Delta t) & \text{if } \omega_{R,z} \leq \omega_{R,y}, \\ \omega_D(t+\Delta t) - \omega_{R,z}(t+\Delta t) & \text{else} \end{cases} \tag{5}$$

Since each component of the rotational optic flow depends on the robot's speed of rotation, we can roughly approximate (for reasons of calculation time) $\omega_{R,y}$ and $\omega_{R,z}$ using angular velocities given by the Inertial Measurement Unit (IMU) of the robot. Note that $\omega_{R,y}$ and $\omega_{R,z}$ depend on the camera position and orientation on the robot. For example, on a downward-facing camera, $\omega_{R,y}$ and $\omega_{R,z}$ can be approximated as the derivatives of the robot's pitch and roll respectively. Rotational optic flow was not considered in [8, 12, 13]. A more complete estimate in real time of $\omega_{R,y}$, $\omega_{R,z}$ and possibly $\omega_{R,x}$ (expressed according to [16]) will be the subject of future studies.
The measured optic flow divergence was filtered to remove outliers.

3. Collision avoidance

3.1. Hypotheses

In this study, we propose controls for a robot of type ROV. Let us define $\mathcal{R}_c = \{O_c, \vec{x}, \vec{y}, \vec{z}\}$ the frame of reference of the camera, where O_c is the center of the camera and $\vec{x}$ corresponds to the optical axis of the camera (see Figure 2.ii). $\vec{x}$ represents the direction in which the optic flow divergence is measured. Let V_x be the velocity of the robot in the direction $\vec{x}$. Since ROVs are holonomic, we consider here that the robot has already a low-level control allowing it to be driven directly in translation on $\vec{x}$: we define u_x the control input in the direction $\vec{x}$. When the autonomous controls described below are not activated, a manual control $u_{x,\text{operator}}$ given by an operator (from a joystick, for example) is applied.

3.2. Emergency braking response

To detect obstacles in an underwater environment, we continuously measured optic flow divergence while an operator remotely controlled the BlueBee robot. When the measured optic flow divergence was lower than an experimentally defined threshold $\omega_{D\,\text{lim}} < 0$ (see Appendix A), we considered that an obstacle was detected and an autonomous emergency braking response was automatically activated. A strong impulse in the opposite direction to the obstacle was imposed on the robot to avoid it. When the obstacle was no longer detected, *i.e.* the divergence became equal to zero or

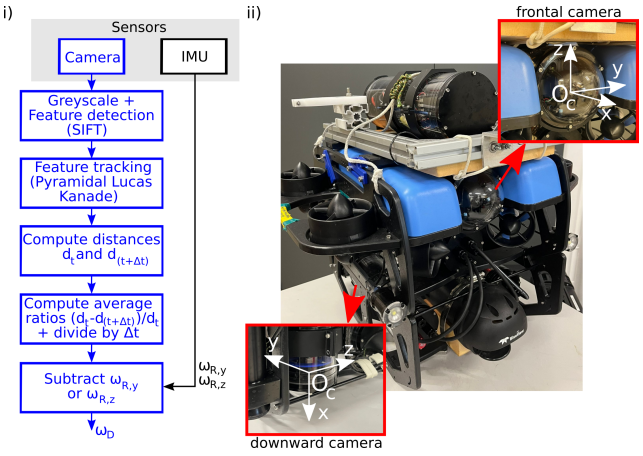

Figure 2: i) Schema of the method used for measuring the optic flow divergence ω_D. ii) The BlueBee robot is equipped with a frontal monocular camera and a downward monocular camera (with their respective coordinate systems $\{O_c, \vec{x}, \vec{y}, \vec{z}\}$).

positive, the robot stopped the motors and then gave back the control to the operator. The robot can so have two behaviors: operator control and emergency braking response.

The emergency braking control can be expressed as:

$$u_x = \begin{cases} -k_v V_x^* & \text{if } m_{\text{braking}}(k) = \text{True} \\ u_{x,\text{operator}} & \text{else} \end{cases} \tag{6}$$

with $m_{\text{braking}}(k)$ the discrete emergency braking variable such that

$$m_{\text{braking}}(k) = \begin{cases} \text{True} & \text{if } \left(\omega_D(t) \leq \omega_{D\,\text{lim}}\right) \\ \text{False} & \text{if } \left(\omega_D(t) \geq 0\right) \\ m_{\text{braking}}(k-1) & \text{else} \end{cases} \tag{7}$$

and where $V_x^* = V_x$ if V_x can be measured or $V_x^* = 1$ otherwise, $k_v > 0$ a design parameter whose value can be high if V_x is unknown.

Note that the knowledge of the velocity V_x is not necessary in the control (6). However, if V_x is known, this information allows a smoother speed-proportional control. Otherwise, a chosen motor impulse strong enough to stop the robot must be chosen.

3.3. Safe-distance maintenance control

Previous authors demonstrated that thanks to the optic flow divergence the state vector $X = [d, V_d]^T$ is locally observable [12, 2]. As a consequence, we can use the measured optic flow divergence to estimate the relative distance d_{est} of the BlueBee robot from the obstacle using an EKF. The EKF receives the optic flow divergence as measurement and the acceleration a_d of the BlueBee robot (given by its IMU) in the direction of the obstacle as input (see Appendix B). In this study, we use the measured optic flow divergence to estimate the relative distance d_{est} of the BlueBee robot from the obstacle after an emergency braking response. d_{est}

is then used to maintain a predefined safe distance.
The safe-distance maintenance control can be expressed as:

$$u_x = -\text{sign}\left(d_{est} - d^*\right) u_{x,\min} \tag{8}$$

where $d^* > 0$ is the desired distance from the obstacle and $u_{x,\min} > 0$ is a control value for a small displacement (see an example for our experiment in Section 4). Note that d^* must be chosen such that optic flow divergence can be measured stably. It can be observed that the control does not use proportional or derivative terms but a constant term. This prevents the robot from converging to the desired distance, thus imposing a small oscillation to continuously measure optic flow divergence and so continuously estimate the relative distance of the BlueBee robot from the obstacle.

4. The BlueBee robot

A BlueROV2[1] was used for tests in a pool, a harbour, a lake and in the sea. BlueROV2 are equipped by standard with a frontal monocular camera, two lights facing forward, a barometer, and an IMU. The BlueBee robot was also equipped with a second monocular camera and two extra lights facing downwards to measure ω_D in that direction and thus use the barometer as ground truth. Both monocular cameras are Low-Light HD USB Camera[2] (standard cameras on BlueROV2), developed for underwater vision with excellent low-light performance, good color handling, and onboard H.264 video compression. An image of size 800×600 was chosen for the transmission. An acoustic camera Blueview[3] was also equipped in the frontal direction to obtain a 2D imaging sonar easy for humans to interpret. Distance extraction is not possible directly on this model.
The Bluerov already has translation commands provided by the MAVROS package. A pwm input must be provided between 1000 and 2000, where 1500 is the neutral input, and 1000 and 2000 are the maximum power in one direction or the other. The pwm input was so expressed as $u_{pwm,x} = u_x + 1500$. Note that motors have a dead-band such that they are inactive if the input is in the interval $u_{pwm,x} \in [1450, 1550]$: we can so choose $u_{x,\min} = 60$. The ROV's downward speed can be accurately measured using the barometer, but the ROV's IMU is not accurate enough to provide forward speed. Thus, we take $V_x^* = V_x$ during downward and $V_x^* = 1$ during frontal testing. We take $\omega_{D\,\text{lim}} = -0.05 rad/s$, $k_v = 400$ and $d^* = 0.7m$. Optic flow divergence and control input were calculated with a frequency of $f = 15$Hz and so $\Delta t = \frac{1}{f}$. The ROV was controlled in depth and heading to keep them constant when the operator did not control them.

5. Experimental Results

A video of the different tests carried out in the pool, harbor, lake and sea is available at the following link:
https://youtu.be/qEFXrTL8Y2k

[1] https://bluerobotics.com/store/rov/bluerov2/
[2] https://bluerobotics.com/store/sensors-cameras/cameras/cam-usb-low-light-r1/
[3] http://www.teledynemarine.com/blueview/

5.1. Tests carried out in a pool

Tests were carried out in the pool of ENSTA Bretagne (in Brest, Brittany, France; shown in Figure 3.i). In order to use the output of the barometer as the ground truth, tests were performed using the monocular camera facing downwards and the bottom of the pool was considered as the obstacle. The downward-facing lights of the BlueBee robot were switched on at maximum.
An example of real-time emergency braking response is shown in Figure 3.iii. The blue section of the curves correspond to the remote operation phase, during which an operator controlled the BlueBee robot with a joystick to descend towards the bottom of the pool. As soon as an optic flow divergence below the given threshold $\omega_{D\,\text{lim}}$ was measured, the emergency braking response (red section of the curves) was automatically activated and the BlueBee robot autonomously moved away from the detected obstacle. We then tested the real-time safe-distance maintenance algorithm under the same conditions. In the example shown in Figure 4, the obstacle was detected at $1.8m$ from the bottom of the pool and thus the BlueBee robot performed an emergency braking stop within $3s$. The EKF was initialized at $1m$ (see Appendix A) and the estimated relative distance d_{est} converged to the ground truth d given by the barometer within $11s$ from the emergency braking response. The average percentage error after convergence $d - d_{est}$ was 5.3%, with a minimum value of -9.52% and a maximum value of 26.84%. d_{est} was used to maintain the BlueBee robot at a predefined safe distance of $0.7m$ from the bottom of the pool. The imposed oscillations (see Figure 4.d) had an average amplitude of approximately $0.2m$.

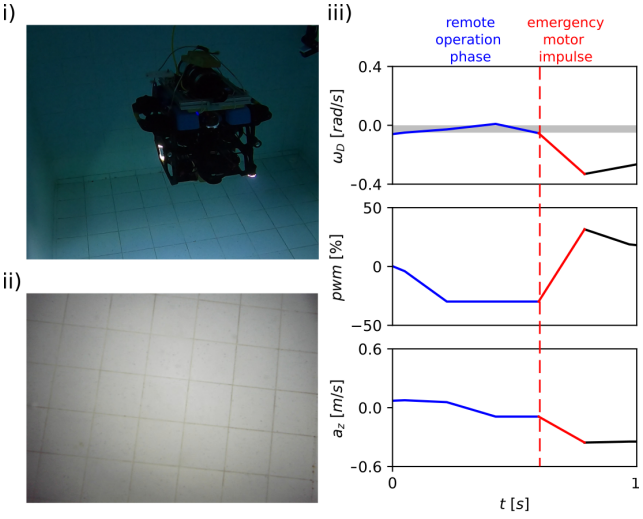

Figure 3: i) The BlueBee robot in the ENSTA Bretagne pool (in Brest, Brittany, France). ii) View of the bottom of the pool from the downward camera. iii) Example of emergency braking response: the BlueBee robot was remotely controlled (in blue) until an optic flow divergence ω_D below the threshold $\omega_{D\,\text{lim}} = -0.05 rad/s$ (gray area) was measured and the autonomous emergency braking response was triggered (in red).

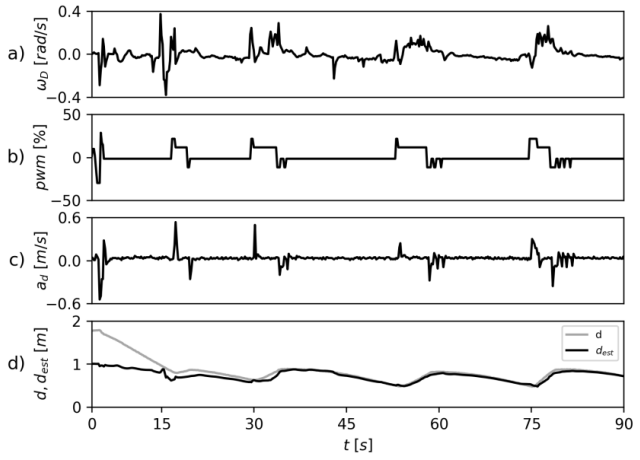

Figure 4: Example of collision avoidance carried out in the ENSTA Bretagne pool (in Brest, Brittany, France): a) measured optic flow divergence ω_D, b) pwm command given to the BlueBee robot, c) acceleration a_d in the direction of the obstacle given by the Inertial Measurement Unit (IMU) of the robot, d) comparison of the estimated relative distance d_{est} with the ground truth d given by the barometer. A video of the tests is available at https://youtu.be/qEFXrTL8Y2k

Similar results were obtained by performing preliminary tests with the frontal camera and considering the side of the pool as an obstacle. Due to the lack of reliability of the equipped sonar in such a confined environment, we lacked a ground truth to validate our results.

5.2. Tests carried out in harbour, lake and sea

5.2.1. Experiments with the downward camera

Real-time safe-distance maintenance tests were carried out in the Moulin Blanc harbour (in Brest, Brittany, France) in salt clear water. Experiments were performed with the downward camera under the same conditions as those carried out in the ENSTA Bretagne pool, with similar results (as shown in Figure 5.A i and ii). The bottom of the harbour was considered as the obstacle to avoid and was detected at a relative distance of about $1.3m$. An emergency braking response was triggered within $3s$, after which the BlueBee robot maintained a safe distance of $0.7m$ from the obstacle.
Tests with the downward camera in fresh water were also carried out in the Guerlédan lake (in Guerlédan, Brittany, France), in the presence of low visibility and high water turbidity. Under these conditions, the method was not effective since the engine's propulsion created dense clouds of particles when the BlueBee robot was close to the bottom of the lake. However, an emergency braking stop could still be performed.

5.2.2. Experiments with the frontal camera and small obstacles

Preliminary tests with the frontal camera in fresh water with low visibility and high turbidity were carried out in the Guerlédan lake (see Figure 5.B.i and ii). Here, the EKF was initialized at $1.5m$ and d^* was $0.8m$. Due to the high turbidity of the water, a Gaussian blur was applied to each frame before measuring the optic flow divergence to filter out floating particles and no further outlier filtering was performed. Although we had no ground truth to validate our results, the real-time safe-distance maintenance algorithm allowed the robot to avoid small and hollow obstacles and maintain a safe distance of $0.8m$.
Additional preliminary tests were performed in the lake to detect a small obstacle in the water column. The obstacle consisted of a red vertical pipe that stood out against the background due to the turbidity of the water (see Figure 6). The pipe was visible in the image captured by the frontal camera from a distance of $1.5m$, but it was only detected later by the optic flow divergence measurement ($< 1m$). However, this was early enough to trigger an effective emergency braking response.
Tests with the frontal camera were also performed in the Mediterranean sea (in Saint-Raphaël, Var, France)[4]. To adapt to visibility and turbidity conditions, the visibility threshold was set at $\omega_{D\,\mathrm{lim}} = -0.4 rad/s$. In the example shown in Figure 7, the obstacle is a reef, occupying only half the camera frame, and detected from a distance of approximately $1.5m$.

6. Discussions and conclusions

While optic flow cues are widely exploited for applications involving UAVs, only a small number of studies have explored their potential for underwater navigation. This is particularly interesting as previous authors have shown that optic flow cues can be measured with commonly available sensors such as monocular cameras [19, 24, 8, 12].
In this study, we present a real-time underwater collision avoidance method based on the optic flow divergence cue measured with a monocular camera. This strategy was tested onboard an ROV (here referred to as BlueBee robot) in a pool, a harbour, a lake and the sea to avoid downward and forward obstacles. The measured optic flow divergence was used to initiate an emergency braking response and then fused with low-cost IMU's outputs to estimate the relative distance of the BlueBee robot from the detected obstacle with an EKF. The estimated relative distance was used to reach a predefined safe distance from the obstacle. The optic flow divergence was then continuously measured thanks to a small imposed oscillation, allowing the robot to maintain the predefined safe distance.
Our experimental results show that optic flow divergence can be used to avoid underwater collisions in real-time to facilitate remote control of an ROV for proximity navigation. This method relies solely on the use of a monocular camera and an IMU, two sensors commonly available on off-the-shelf ROVs. Additionally, the presented approach to measuring optic flow divergence has the advantage of requiring low computational resources compared to other methods (such as DNN). No transformation of the perceived image

[4] during Submeeting 2024: https://submeeting2024.univ-tln.fr/

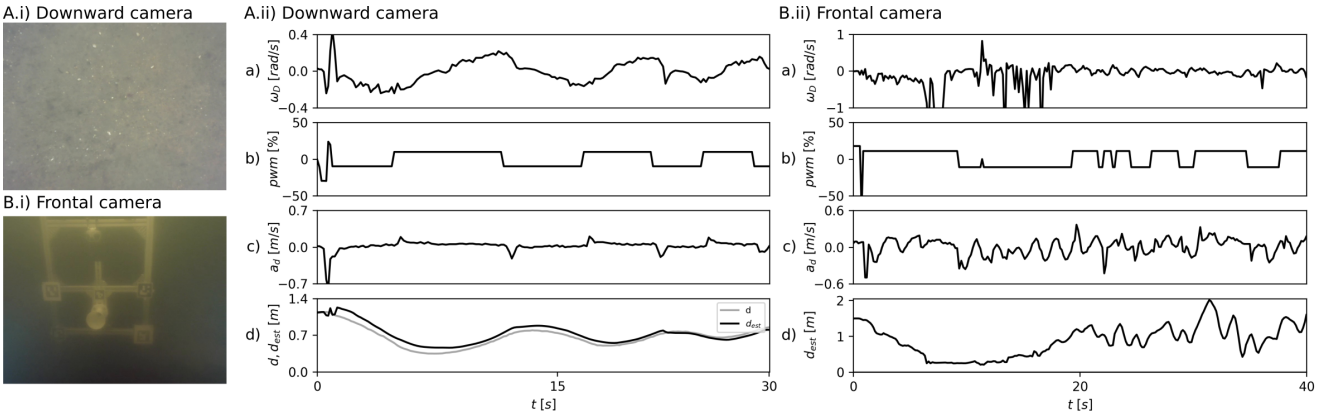

Figure 5: A) Test carried out in the Moulin Blanc harbour (in Brest, Brittany, France): A.i) view from the downward camera, A.ii) a) measured optic flow divergence ω_D, b) pwm command given to the robot, c) acceleration a_d in the direction of the obstacle given by the Inertial Measurement Unit (IMU) of the robot, d) comparison of the estimated relative distance d_{est} with the ground truth d given by the barometer. B) Test carried out in the Guerlédan lake (in Guerlédan, Brittany, France): A.i) view from the frontal camera, showing a hollow obstacle; A.ii) preliminary results. A video of the tests is available at https://youtu.be/qEFXrTL8Y2k .

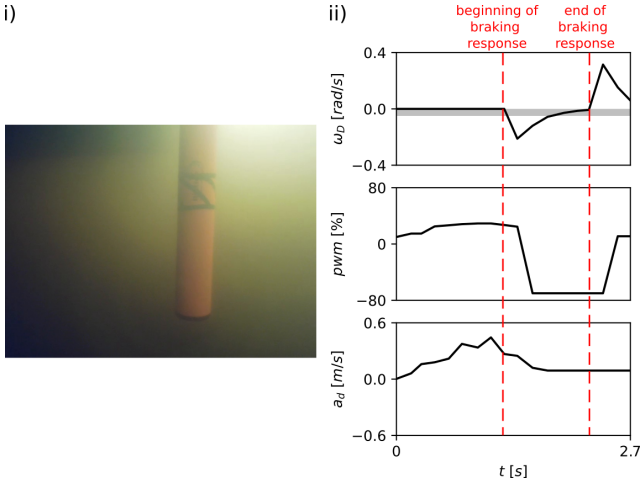

Figure 6: Test carried out in the Guerlédan lake (in Guerlédan, Brittany, France): i) view from the frontal camera showing an obstacle in the water column, ii) preliminary results of emergency breaking response. A video of the tests is available at https://youtu.be/qEFXrTL8Y2k .

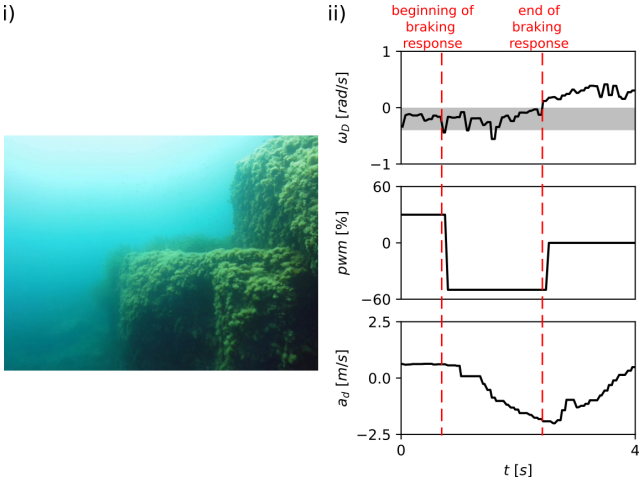

Figure 7: Test carried out in the Mediterranean sea (in Saint-Raphaël, Var, France): i) view from the frontal camera showing the obstacle, ii) preliminary results of emergency breaking response. A video of the tests is available at https://youtu.be/qEFXrTL8Y2k .

is necessary to compensate for camera rotation movements: only a rough approximation of the highest component of the rotational optic flow is subtracted from the optic flow divergence. The method presented in this study is better suited to obstacles in close proximity and can therefore be considered as complementary to sonar in the distance range where sonar could be too affected by reverberation.

Our results show that this strategy works even in the presence of high water turbidity and low visibility. By using a Gaussian filter to attenuate the effect of floating particles, obstacles tend to be easily detected since they are the only source of clear visual information. However, under these conditions obstacles tend to be detected when they are already quite close to the ROV. Therefore, this method is more suitable for applications involving low speeds. More generally, the use of optic flow requires slow movements to obtain good measurements of the optic flow divergence under such visibility conditions.

Future work will include a further analysis of each component of the rotational optic flow (expressed according to [16]) to improve their estimates and thus better measure the optic flow divergence. Future work will also include the development of a strategy based on a combination of optic flow divergence and translational optic flow to cross the detected obstacle after an emergency braking response. As the optic flow divergence allows the BlueBee robot to

maintain a safe distance from the obstacle in order to avoid collisions, we could consider using a similar technique to detect and follow a surface at a given distance based solely on optic flow cues (for dam inspection, for example). In this study we measured the overall optic flow divergence over the entire captured image, without considering that different surfaces and obstacles might be at different relative distances from the robot. Future work will explore how to apply this approach to the presence of multiple obstacles at different distances from the ROV. In addition, in this study we consider only fixed obstacles. Future work will include the application of this algorithm to the case of moving obstacles. Future work will also include testing this approach for an Unmanned Surface Vehicle to perform avoidance of both fixed and moving obstacles.

Acknowledgments

The participation of L.B. was supported by Région Bretagne and BPI France via the EXOS 2024 project. L.B thanks PIXEL sur MER (in particular Dr. J. Damers) and SEA.AI for their support. The participation of C.V. was supported by CNRS (Centre national de la recherche scientifique). L.B, C.V. and L.J. were also supported by ENSTA Bretagne (École nationale supérieure de techniques avancées Bretagne). The authors would like to thank the organisers of Submeeting 2024, during which tests were carried out in the Mediterranean Sea. The authors are also grateful to the two anonymous referees, whose suggestions helped to greatly improve the manuscript.

A. Visibility threshold

A test was carried out in the ENSTA Bretagne pool to determine the threshold below which the measured optic flow divergence can be considered an indicator of the presence of an obstacle. The BlueBee robot moved from the bottom of the pool to the surface and the barometer was used to measure its relative distance d from the bottom of the pool. The optic flow divergence was measured using the downward monocular camera with the robot's downward-facing lights switched on at maximum. Figure 8.a shows that from a distance d of about $1m$ from the bottom of the pool the measured optic flow divergence ranges around $0rad/s$, indicating that the obstacle is no longer detected under these conditions. A test in which the robot descended from the surface to the bottom of the pool showed similar results (see Figure 8.b). To increase the robustness to noise, we chose a threshold $\omega_{D\,\mathrm{lim}} = -0.05rad/s$.

B. Extended Kalman Filter

The BlueBee robot was modeled in the form of a double integrator receiving as input the acceleration in the direction of the obstacle a_d given by its IMU. The robot's state space

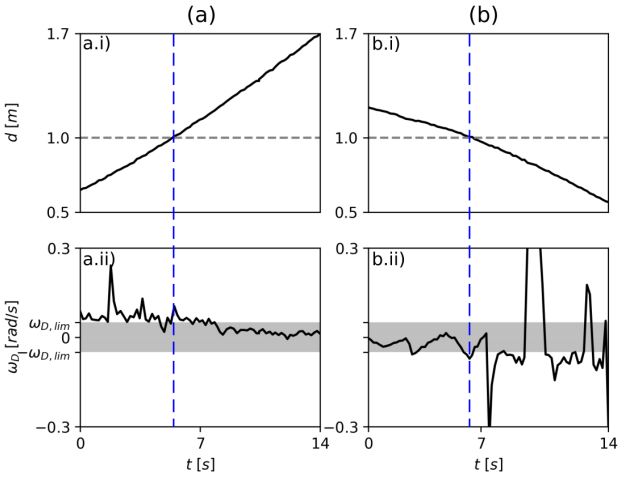

Figure 8: Tests in which the BlueBee robot moves from the bottom of the pool to the surface (a) and descends from the surface to the bottom of the pool (b) respectively. (a.i and b.i) Distance d of the robot from the bottom of the pool given by the barometer. Only the time interval between $0s$ and $14s$ is shown, corresponding to the robot crossing the $1m$ threshold (dashed blue line). (a.ii and b.ii) Measured optic flow divergence ω_D (in black) and area bounded by the thresholds $\pm\omega_{D\,\mathrm{lim}}$ (in grey).

representation can therefore be expressed as:

$$\begin{cases} \dot{X} = f(X, a_d) = A \cdot X + B \cdot a_d = \begin{bmatrix} 0 & 1 \\ 0 & 0 \end{bmatrix} \cdot X + \begin{bmatrix} 0 \\ 1 \end{bmatrix} \cdot a_d \\ Y = g(X) = [X(2)/X(1)] = V_d/d = \omega_D \end{cases} \tag{9}$$

where $X = \left[d, V_d\right]^T$ is the ROV's state vector. The discretized model of the BlueBee robot used in the EKF calculations can be expressed as:

$$\begin{cases} X[k+1] = \Phi \cdot X[k] + \Gamma \cdot U[k] \\ Y[k] = C_k \cdot X[k] + D_k \cdot U[k] \end{cases} \tag{10}$$

with

$$\Phi = e^{A \cdot dt} \tag{11}$$

$$\Gamma = \left(\int_0^{dt} e^{A \cdot \tau} d\tau\right) \cdot B \approx dt \cdot B \tag{12}$$

$$C_k = g(X_k) = \left[\frac{X_2[k]}{X_1[k]}\right] = \left[\frac{V_d[k]}{d[k]}\right] \tag{13}$$

$$D_k = 0 \tag{14}$$

where dt is the discretization time.

References

[1] L. Bergantin, C. Coquet, J. Dumon, A. Negre, T. Raharijaona, N. Marchand, and F. Ruffier. Indoor and outdoor in-flight odometry based solely on optic flows with oscillatory trajectories. *International Journal of Micro Air Vehicles*, page 15, 2023.

[2] L. Bergantin, N. Harbaoui, T. Raharijaona, and F. Ruffier. Oscillations make a self-scaled model for honeybees' visual odometer reliable regardless of flight trajectory. *Journal of the Royal Society Interface*, 18(182):20210567, 2021.

[3] J.-Y. Bouguet et al. Pyramidal implementation of the affine lucas kanade feature tracker description of the algorithm. *Intel corporation*, 5(1-10):4, 2001.

[4] F. Boyer, V. Lebastard, S. Ferrer, and F. Geffard. Underwater pretouch based on artificial electric sense. *The International Journal of Robotics Research*, 39(6):729–752, 2020.

[5] A. Bucci, L. Zacchini, M. Franchi, A. Ridolfi, and B. Allotta. Comparison of feature detection and outlier removal strategies in a mono visual odometry algorithm for underwater navigation. *Applied Ocean Research*, 118:102961, 2022.

[6] A. Burton and J. Radford. *Thinking in perspective: critical essays in the study of thought processes*. Taylor & Francis, 2022.

[7] V. Creuze. Monocular odometry for underwater vehicles with online estimation of the scale factor. In *IFAC 2017 World Congress*, 2017.

[8] G. de Croon. Monocular distance estimation with optical flow maneuvers and efference copies: a stability-based strategy. *Bioinspiration & biomimetics*, 11(1):016004, 2016.

[9] F. Expert and F. Ruffier. Flying over uneven moving terrain based on optic-flow cues without any need for reference frames or accelerometers. *Bioinspiration and Biomimetics*, 10, 2015.

[10] A. Ferone, M. Lazzaro, V.M. Scarrica, A. Ciaramella, and A. Staiano. *A Synthetic Dataset for Learning Optical Flow in Underwater Environment*, pages 147–156. Springer Nature Singapore, Singapore, 2023.

[11] B. Herissé, T. Hamel, R. Mahony, and F.-X. Russotto. Landing a vtol unmanned aerial vehicle on a moving platform using optical flow. *IEEE Transactions on robotics*, 28(1):77–89, 2011.

[12] H. W. Ho, G. de Croon, and Q. Chu. Distance and velocity estimation using optical flow from a monocular camera. *International Journal of Micro Air Vehicles*, 9(3):198–208, 2017.

[13] H. W. Ho, G. de Croon, E. Van Kampen, Q. P. Chu, and M. Mulder. Adaptive gain control strategy for constant optical flow divergence landing. *IEEE Transactions on Robotics*, 34(2):508–516, 2018.

[14] F. Iida. Biologically inspired visual odometer for navigation of a flying robot. *Robotics and autonomous systems*, 44(3-4):201–208, 2003.

[15] F. Kendoul, I. Fantoni, and K. Nonami. Optic flow-based vision system for autonomous 3d localization and control of small aerial vehicles. *Robotics and autonomous systems*, 57(6-7):591–602, 2009.

[16] J.J. Koenderink and A.J. van Doorn. Facts on optic flow. *Biological Cybernetics*, 56:247–254, 1987.

[17] D. G. Lowe. Object recognition from local scale-invariant features. In *Proceedings of the seventh IEEE international conference on computer vision*, volume 2, pages 1150–1157. Ieee, 1999.

[18] D. G. Lowe. Distinctive image features from scale-invariant keypoints. *International journal of computer vision*, 60:91–110, 2004.

[19] B. D. Lucas and T. Kanade. An iterative image registration technique with an application to stereo vision. In *IJCAI'81: 7th international joint conference on Artificial intelligence*, volume 2, pages 674–679, 1981.

[20] P.A. Miller, J.A. Farrell, Y. Zhao, and V. Djapic. Autonomous underwater vehicle navigation. *IEEE Journal of Oceanic Engineering*, 35(3):663–678, 2010.

[21] R.C. Nelson and J. Aloimonos. Obstacle avoidance using flow field divergence. *IEEE Transactions on Pattern Analysis and Machine Intelligence*, 11(10):1102–1106, 1989.

[22] F. Ruffier and N. Franceschini. Optic flow regulation: the key to aircraft automatic guidance. *Robotics and Autonomous Systems*, 50(4):177–194, 2005.

[23] H. Teigland, V. Hassani, and M. T. Møller. Operator focused automation of rov operations. In *2020 IEEE/OES Autonomous Underwater Vehicles Symposium (AUV)*, pages 1–7, 2020.

[24] F. Van Breugel, K. Morgansen, and M. H Dickinson. Monocular distance estimation from optic flow during active landing maneuvers. *Bioinspiration & biomimetics*, 9(2):025002, 2014.

[25] P. Xia, H. You, and J. Du. Visual-haptic feedback for rov subsea navigation control. *Automation in Construction*, 154:104987, 2023.

[26] F. Xiao, P. Zheng, J. Di Tria, B.B. Kocer, and M. Kovac. Optic flow-based reactive collision prevention for mavs using the fictitious obstacle hypothesis. *IEEE Robotics and Automation Letters*, 6(2):3144–3151, 2021.

[27] Z. Xu, M. Haroutunian, A.J. Murphy, J. Neasham, and R. Norman. An underwater visual navigation method based on multiple aruco markers. *Journal of Marine Science and Engineering*, 9(12):1432, 2021.

[28] B. Zhang, D. Ji, S. Liu, X. Zhu, and W. Xu. Autonomous underwater vehicle navigation: a review. *Ocean Engineering*, page 113861, 2023.

[29] S. Zhang, S. Zhao, D. An, J. Liu, H. Wang, Y. Feng, D. Li, and R. Zhao. Visual slam for underwater vehicles: A survey. *Computer Science Review*, 46:100510, 2022.